frontiers | Frontiers in Marine Science

TYPE Original Research
PUBLISHED 26 August 2024
DOI 10.3389/fmars.2024.1451624

OPEN ACCESS

EDITED BY
Fei Li,
Southwest Petroleum University, China

REVIEWED BY
Zhou Wang,
China University of Geosciences Wuhan, China
Tingting Chen,
University of Science and Technology of China, China

*CORRESPONDENCE
Xiaoming Miao
xiaomingmr1992@126.com
Kailong Gan
gankl@hn-dstic.com

RECEIVED 19 June 2024
ACCEPTED 29 July 2024
PUBLISHED 26 August 2024

CITATION
Wei J, Miao X, Gan K, Li J, Li J, Liu X, Xu H, Chen S, Ta K, Wan Z and Wu T (2024) The formation of tubular seep carbonate deciphered from mineralogical and geochemical characteristics: an example from the South China Sea. *Front. Mar. Sci.* 11:1451624. doi: 10.3389/fmars.2024.1451624

The formation of tubular seep carbonate deciphered from mineralogical and geochemical characteristics: an example from the South China Sea

Jiangong Wei[1,2,3], Xiaoming Miao[4]*, Kailong Gan[5]*, Jiangtao Li[6], Jiwei Li[7], Xiting Liu[4], Hengchao Xu[7], Shun Chen[7], Kaiwen Ta[7], Zhifeng Wan[8] and Tingting Wu[2]

[1]Sanya Institute of South China Sea Geology, Guangzhou Marine Geological Survey, Sanya, China, [2]MLR Key Laboratory of Marine Mineral Resources, Guangzhou Marine Geological Survey, Guangzhou, China, [3]Academy of South China Sea Geological Science, China Geological Survey, Sanya, China, [4]Key Lab of Submarine Geosciences and Prospecting Technology, MOE, College of Marine Geosciences, Ocean University of China, Qingdao, China, [5]Hainan Deep-Sea Technology Innovation Center, Sanya, China, [6]State Key Laboratory of Marine Geology, Tongji University, Shanghai, China, [7]Deep Sea Science Division, Institute of Deep Sea Science and Engineering, Chinese Academy of Sciences, Sanya, China, [8]School of Marine Sciences, Sun Yat-sen University/Southern Marine Science and Engineering Guangdong Laboratory (Zhuhai), Zhuhai, China

As a special type of seep carbonate, the many details concerning the formation mode and mechanism of tubular seep carbonates are rarely reported. Here, new geochemical and mineralogical data regarding tubular seep carbonate (SQW-65) are reported. Sample SQW-65 had anomalously negative $\delta^{13}C$ values and positive $\delta^{18}O$ values, which suggested the dissociation of gas hydrate. Additionally, almost all the sub-samples showed no Ce anomaly ($Ce/Ce^*_{average}$ = 0.93), with obvious U enrichment (21.3< U_{EF} <240.3), which indicates that the studied tubular seep carbonate was formed in an anoxic environment. Subsequently, the formation process of the studied tubular seep carbonate is further discussed according to the variability of mineralogical and geochemical characteristics from the rim to the core of the tubular formation. In the early stage of the studied tubular seep carbonate (periphery), owing to the influence of terrigenous components, the quartz and Ti content and Y/Ho ratio were high. However, with the formation of the periphery, the influence of terrigenous components was gradually weakened. In addition, from the rim to the core, the carbon and oxygen isotope values showed a "covariation" coupling relationship, an enrichment of U, and a reduction in total rare earth element content. This is because as the outer wall thickens and the internal fluid channel narrows, the intensity of the sulphate-driven anaerobic oxidation of methane and the associated precipitation rate of carbonate also increase.

KEYWORDS

tubular seep carbonates, SD-AOM, methane seep, South China Sea, trace elements

1 Introduction

Seep carbonate is a special authigenic carbonate that is common in methane-rich fluid seep areas of active and passive continental margins (Peckmann et al., 2001; Han et al., 2008; Ge et al., 2010; Feng and Chen, 2015; Feng et al., 2016, 2018; Bayon et al., 2013; Tong et al., 2013; Hu et al., 2014; Smrzka et al., 2020, 2021; Wei et al., 2020, 2022, 2023; Liang et al., 2022). Research revealed that ascending methane and infiltrating sulphate meet near the sulphate methane transition zone (SMTZ), where approximately 80 to 90% of the methane is consumed by microorganisms through the sulphate-driven anaerobic oxidation of methane (SD-AOM, Boetius et al., 2000; Saunois et al., 2016). In the course of SD-AOM, HCO_3^- is generated and can further react with the dissolved Ca^{2+} and Mg^{2+} to form authigenic carbonate minerals (Hill et al., 2004; Joseph et al., 2013). Therefore, authigenic carbonates formed in SMTZ are regarded as an excellent archive of methane seep activity in geological history and play a significant role in the study of the properties and evolution of continental margin seep fluids (Hu et al., 2014; Feng and Chen, 2015; Wang et al., 2015; Zwicker et al., 2015; Smrzka et al., 2020, 2021). Additionally, large-scale gas hydrate dissociation can easily cause regional and even global environmental and ecological disasters, such as ocean hypoxia, biological extinction, and global warming (Dickens et al., 1997; Hesselbo et al., 2000; Kennett James et al., 2000; Ruppel and Kessler, 2017; Chen et al., 2019; Deng et al., 2021; Wei et al., 2020, 2022; Liu et al., 2024). Therefore, research on cold seeps can help us better understand the relationship between global climate and environmental change and methane seep activities (Deng et al., 2021; Wei et al., 2020, 2022), and provide a reference for solving global problems such as climate warming.

So far, seep carbonates around the world have complex morphological characteristics. They are often formed in shallow surface sediments with different forms, such as crusts, nodules, chimneys, chemical reefs, mounds, and veins (Bayon et al., 2013; Bian et al., 2013; Wang et al., 2015; Argentino et al., 2019), and they even protrude from the seafloor extending into the bottom seawater to form huge carbonate buildup (Han et al., 2008). Moreover, it has been shown that the different morphologies of carbonates record the evolution of seep intensity, depositional environment, precipitation rate, and chemical composition of seep fluids (Bayon et al., 2013; Feng et al., 2018; Smrzka et al., 2020, 2021; Jin et al., 2021). Tubular carbonates, which form around methane seep fluid channels in the sediment, are common in modern and ancient cold-seep environments around the world, such as the northern South China Sea (Han et al., 2013; Yang et al., 2018; Jin et al., 2021), Mediterranean Sea (Bayon et al., 2013), Campos Basin (offshore Brazil) (Wirsig et al., 2012), Krishna-Godavari Basin (offshore India) (Mazumdar et al., 2009; Joshi et al., 2014), Enza River field in the Northern Apennines in Italy (Oppo et al., 2015), and Hikurangi Margin in New Zealand (Campbell et al., 2008). It is believed that tubular carbonates are formed when the fluid seep flux is vigorous or at least highly focused (Liang et al., 2022). Oppo et al. (2015), and that they act as a focused SMTZ in methane-rich pore fluids in sediments. In addition, although some tubular carbonates reflect episodic oxidation environments (Liang et al., 2022), most are formed in anoxic environments (Yang et al., 2018; Jin et al., 2021).

It is obvious that many studies have regarded tubular carbonates as a whole, and have not fully considered the specific effects of different stages of cold seep activity on their mineralogy and geochemical characteristics (Han et al., 2008, 2013, 2014). This not only greatly restricts our understanding of the formation mechanism and model of tubular carbonates (Wirsig et al., 2012; Bayon et al., 2013; Yang et al., 2018) but also may provide misleading information when we use tubular carbonates to reconstruct ancient marine environments (Jin et al., 2021; Huang et al., 2022). However, the mineralogy and geochemistry of cold seep carbonates usually contain abundant information about cold seep activities (Feng et al., 2018; Smrzka et al., 2020, 2021). Therefore, we believe that the evolution of the mineralogical and geochemical characteristics of tubular seep carbonates may have a unique regularity during their formation. This study aimed to reconstruct the formation mechanism and model of tubular seep carbonates through the systematic sampling of carbonate samples from the rim to the core of the tubular formation (the Dongsha area in the South China Sea, Figure 1) for geochemical and mineralogical analyses.

2 Geological setting

As one of the largest marginal seas in the Western Pacific, the South China Sea is controlled by the complex interaction of the Eurasian plate, Pacific Plate, and Indo-Australian plate (Taylor and Hayes, 1980; Suess, 2005). Tectonically, the northern South China Sea is a passive continental margin formed during the Middle Oligocene and Early Miocene (32–17 Ma). The region contains a succession of sedimentary basins (such as the Qiongdongnan Basin and Pearl River Mouth Basin) with thick sedimentary sequences and fast deposition rates (Taylor and Hayes, 1980; Xie et al., 2006; Liu et al., 2016). Moreover, the extensive development of faults and mud diapirs the northern South China Sea is conducive to the flow of methane-rich fluids (Suess, 2005). In 2004, different types of seep carbonates were discovered during the Chinese-German RV SONNE Cruise 177 in the northeastern part of the Dongsha area (Han et al., 2008). Therefore, the Dongsha area of the South China Sea has become an excellent target area for the study of cold seep activities.

3 Materials and methods

In 2018, a joint scientific expedition was conducted using the Institute of Deep Sea Science and Engineering's manned submersible "Shenhaiyongshi" and R/V "Tansuoyihao" (Wei et al., 2023). The tubular seep carbonates (SQW-65) were recovered from the seafloor

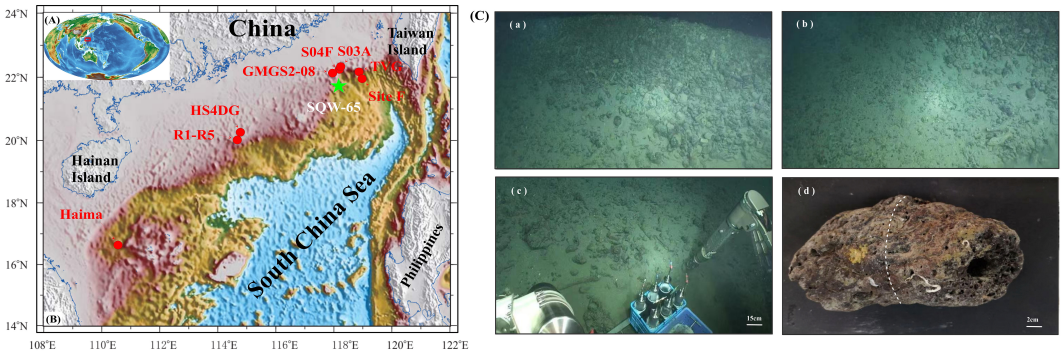

FIGURE 1
(A) Map of the world. The rectangle (red) represents the study area **(B)**. **(B)** Core locations on the northern slope of the South China Sea. The green star represents the research core and the red circles represent the reference cores. SQW-65 (this study), Jiulong methane reef (TVG, Han et al., 2008; Ge et al., 2020), S03A and S04F (Yang et al., 2018), GMGS2-08 (Deng et al., 2021), Site F (Feng and Chen, 2015), Haima (ROV1and ROV2, Liang et al., 2017), Shenhu (HS4DG, Tong et al., 2013, Ge et al., 2020; R1-R5, Liang et al., 2022). **(C)**, Seafloor observations at SQW-65 (a–d).

at a depth of 500 m in the Dongsha area, using the manned submersible "Shenhaiyongshi" (Figures 1, 2). The bottom water temperature was 8.2°C. The carbonate samples were described, photographed, and sampled for further analysis at room temperature in the laboratory.

An XRD with an *in situ* microzone analysis function was used to identify mineral components. The experiment was completed in the Guangdong Provincial Key Laboratory of Marine Resources and Coastal Engineering, following the procedure described by Wei et al. (2023). The measurements were obtained using a Rigaku Rapid II X-ray diffraction system (Mo Kα radiation). The working voltage was 50 kV, the current was 30 mA, the incident beam spot diameter was 0.1 mm, and the exposure time was 5 min. Moreover, mineral phases were identified and quantitatively calculated using PDXL2 software according to the method described by Rietveld (1967).

The carbon and oxygen stable isotope compositions of the tubular seep carbonates were analyzed at the Guangdong Provincial Key Laboratory of Marine Resources and Coastal Engineering using a Thermo MAT-253 isotope ratio mass spectrometer. Each sample produces 10 peaks of the mass spectrum, and the average value is the isotopic value of the sample. The results are given in the standard δ-notation in per mil (‰) relative to the Vienna Peedee Belemnite Standard (V-PDB).

Element analysis of the tubular seep carbonates used an Agilent 7700e ICP-MS at the Wuhan SampleSolution Analytical Technology Co., Ltd., Wuhan, China. Powdered samples were treated with 5% acetic acid solutions for element analyses of tubular seep carbonates.

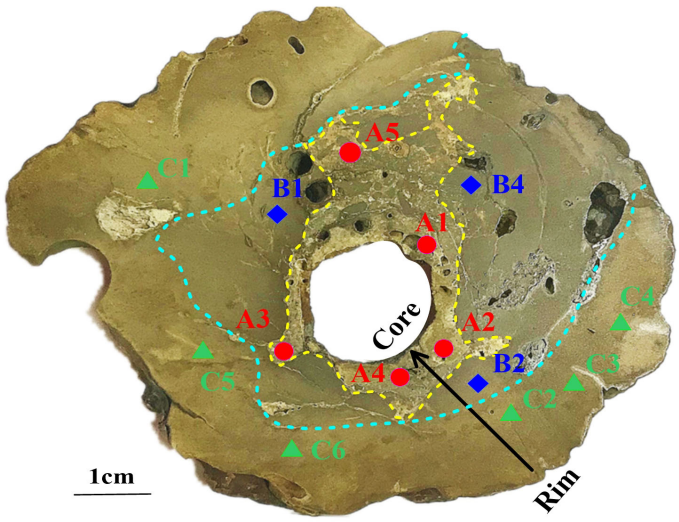

FIGURE 2
Photographs of the tubular seep carbonate SQW-65. The dashed blue line represents the dividing line between zones B and C. The dashed yellow line represents the dividing line between zones B and A. The sampling locations are indicated by circles (red), triangles (green), and diamonds (blue).

Strontium isotope compositions of the tubular seep carbonates were analyzed at the Wuhan Sample Solution Analytical Technology Co., Ltd, using a Neptune Plus MC-ICP-MS (Thermo Fisher Scientific, Dreieich, Germany). While analyzing the samples, the international NIST 987 was used to monitor the status of the instrument every seven samples. All Sr isotope ratios were obtained using "Iso-Compass" software (Zhang et al., 2020). In addition, the USGS reference materials BCR-2 (basalt) and RGM-2 (rhyolite) yielded results of 0.705012 ± 22 (2SD, n=63) and 0.704173 ± 20 (2SD, n=20) for $^{87}Sr/^{86}Sr$, respectively, which is identical, within error, to their published values (Li et al., 2012; Zhang and Hu, 2020).

4 Results

4.1 Mineralogical and petrographic description

Using the manned submersible "Shenhaiyongshi", the existence of extensive and massive carbonate deposits was confirmed (Figure 1C). These carbonates were distributed sporadically in different shapes and sizes, with a gray and dark brown color (Figure 1C). The maximum diameter of the obtained tubular seep-carbonates (SQW-65) measured approximately 10 cm, and the channel exhibited a diameter of approximately 2 cm (Figure 1C). The tubular seep carbonate was cleaned with deionized water and air-dried and cut in half along its maximum diameter. From its cross-section, we could see three distinct colors. The color was lightest near the channel, and darkest on the periphery. Furthermore, based on the color variation, the cross-section of the tubular seep carbonate was categorized into three distinct regions from the inner to the outer periphery, designated as Areas A, B, and C (Figure 2).

The XRD results revealed that carbonate and quartz were the main mineral components of the carbonate samples of SQW-65 (Figure 3; Supplementary Table S1), the contents of which were 49.4% to 91.1% (average of 71.9%) and 8.9% to 50.6% (average of 28.1%), respectively.

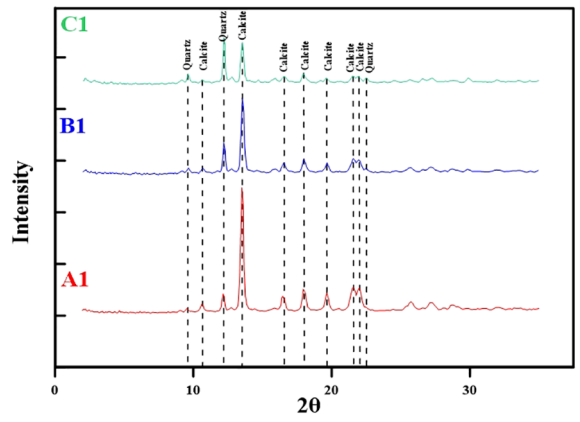

FIGURE 3
Partial X-ray diffraction images of SQW-65.

The samples showed a trend of decreasing carbonate content from the periphery to the inner portion of the tubular seep carbonate, whereas the quartz content increases (Figure 3).

4.2 Carbon and oxygen isotopes

The carbon and oxygen stable isotopic composition of the tubular seep carbonate (SQW-65) is reported in Supplementary Table S2. The $\delta^{13}C$ values of SQW-65 varied from −42.6‰ to −33.2‰ (average of −38.3‰, n=14, Figure 4), with a small variation. The $\delta^{18}O$ values of SQW-65 varied from 0.30 to 2.3‰ (average of 1.3‰, n=14, Figure 4).

4.3 Strontium isotope

The strontium isotope composition of the tubular seep carbonate (SQW-65) is reported in Supplementary Table S2. The $^{87}Sr/^{86}Sr$ ratio values of SQW-65 varied from 0.709139 to 0.709297 (average 0.709246, n=13, Figure 5). These values are similar to those of modern seawater (0.709175, Paytan et al., 1993).

4.4 Major, trace, and rare earth elements

The major and trace elements composition of the tubular seep carbonate (SQW-65) is reported in Supplementary Tables S3, S4. The concentrations of Al and Ti in the sample (n=13, Figure 6) ranged from 1,018 to 1,764 ppm and from 3.6 to 10.0 ppm, respectively. The redox-sensitive element U ranged from 0.9 to

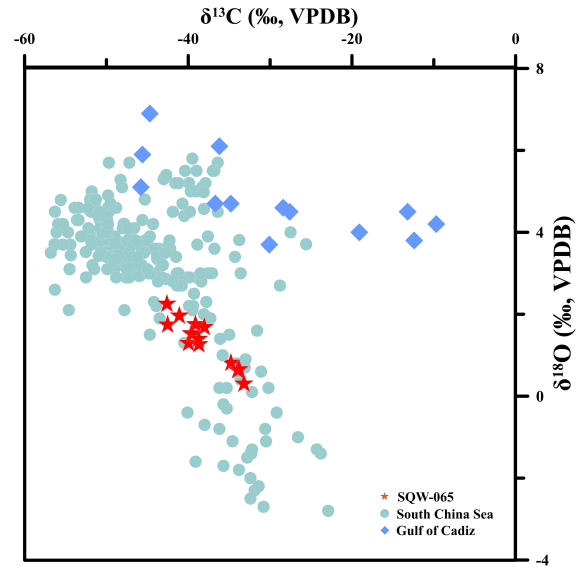

FIGURE 4
Carbon and oxygen isotopic compositions of seep carbonates: SQW-65 (this study), the South China Sea (TVG, Han et al., 2008; Ge et al., 2020; S03A and S04F, Yang et al., 2018; GMGS2-08, Deng et al., 2021; Site F, Feng and Chen, 2015; ROV1and ROV2, Liang et al., 2017; HS4DG, Tong et al., 2013, Ge et al., 2020; R1-R5, Liang et al., 2022), Gulf of Cadiz (Wang et al., 2015).

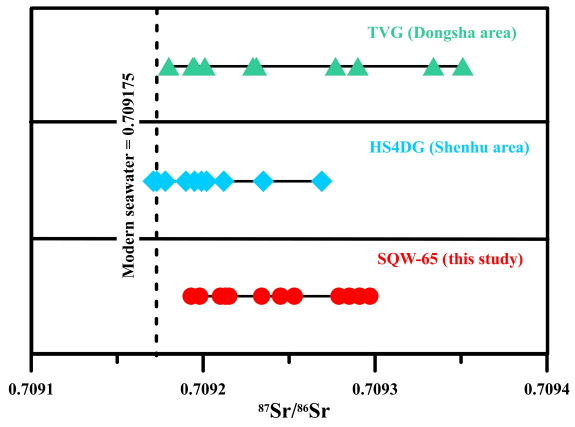

FIGURE 5
$^{87}Sr/^{86}Sr$ ratios of authigenic carbonates from site SQW-65. The dashed line corresponds to the $^{87}Sr/^{86}Sr$ ratio of modern seawater (0.709175, Paytan et al., 1993). Dongsha (Ge et al., 2020), Shenhu (Ge et al., 2020), SQW-65 (this study).

10.3 ppm in the sample (n=13, Figure 6). The enrichment factor of U is calculated as $X_{EF} = [(X/Al)_{sample}/(X/Al)_{PAAS}]$, which is normalized using the Post-Archean Australian Shale (PAAS, Taylor and McLennan, 1985). A trend of increasing U_{EF} occurred from the periphery inward in the samples.

The rare earth element (REE) composition of the tubular seep carbonate (SQW-65) is reported in Supplementary Table S2. The REE contents were normalized against the PAAS (Taylor and McLennan, 1985). The shale-normalized REE patterns of samples did not exhibit Ce anomalies ($Ce/Ce^*_{average} = 0.93$) and middle REE (MREE) enrichment (n=13, Figure 6). In this study, $Ce/Ce^* = 3Ce_N/(2La_N + Nd_N)$ and $Pr/Pr^* = 2Pr_N/(Ce_N + Nd_N)$, where N refers to the normalization of the concentration against the PAAS (Taylor and McLennan, 1985).

5 Discussion

5.1 Fluid sources and environmental conditions

The stable isotopic composition of carbon and oxygen in seep carbonates is important in revealing the composition and source of seeping fluids (Kim and O'Neil, 1997; Peckmann et al., 2001; Kim et al., 2007; Bayon et al., 2013; Feng et al., 2018; Wei et al., 2020, 2022). The formation of methane has been demonstrated to exhibit a preferential utilization of ^{12}C, leading to a significantly reduced $\delta^{13}C$ value in general (−110 to −30‰, Sackett, 1978; Whiticar, 1999). Therefore, when sulfate-driven anaerobic oxidation of methane occurs, the carbon sources of ^{13}C-poor will eventually be transferred to cold seep carbonates, resulting in obvious carbon isotope differences between cold seep carbonates and normal marine carbonates (Peckmann et al., 2001; Peckmann and Thiel, 2004). As shown in Figure 3, the carbon isotope values of the tubular seep carbonate (SQW-65) in this study ranged from −43.6 to −33.2‰, which is very similar to the carbon isotope composition of seep carbonates in other parts of the world, such as the Gulf of Cadiz, Qiongsoutheast Sea, and Shenhu Sea (Han et al., 2008; Tong et al., 2013; Feng and Chen, 2015; Wang et al., 2015; Liang et al., 2017; Deng et al., 2021; Wei et al., 2020, 2022). Moreover, these results also reflect that methane has proven to be thermogenic in origin, or a mixture of thermogenic and biogenic methane, which is consistent with previous studies (Deng et al., 2021; Huang et al., 2022).

The $\delta^{18}O$ values of seep carbonates are primarily influenced by the oxygen isotopic composition of the precipitating fluid and the temperature conditions at the time of formation (Kim and O'Neil, 1997; Kim et al., 2007; Feng and Chen, 2015; Liang et al., 2017). Therefore, the oxygen isotope composition of seep carbonates can reflect the information of the fluid source and temperature during

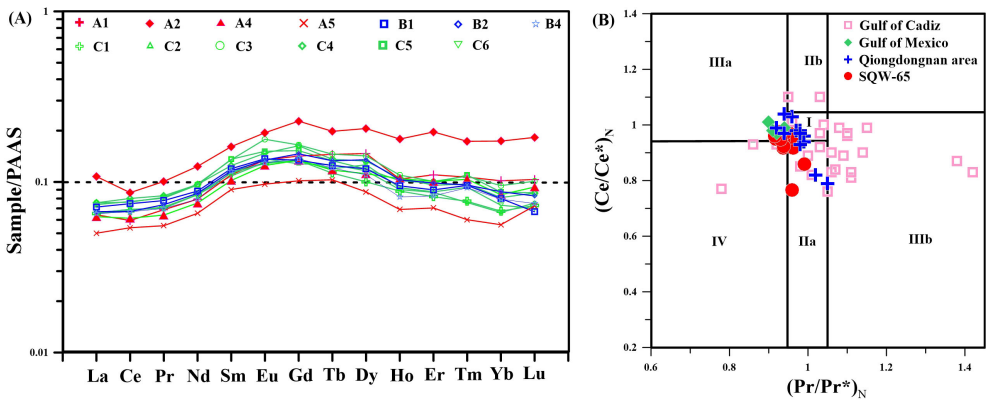

FIGURE 6
(A) Shale-normalized REE distribution patterns of the carbonate. PAAS, Post-Archean Australian Shale (Taylor and McLennan, 1985). **(B)** Ce/Ce* vs. Pr/Pr* diagram [after Bau and Dulski (1996)] of authigenic carbonate samples. Field I - no anomaly; field IIa - positive La anomaly produces an apparent negative Ce anomaly; field IIb - a negative La anomaly causes an apparent positive Ce anomaly; field IIIa - real positive Ce anomaly; field IIIb - real negative Ce anomaly; field IV - positive La anomaly disguises a positive Ce anomaly.

the precipitation of authigenic carbonates. In seep environments, abnormally positive $\delta^{18}O$ values of seep carbonates have been widely found. This is because when gas hydrate dissociation occurs, the ^{18}O-enriched fluids released by the hydrate participates in the precipitation process of the carbonates, and ultimately changes the oxygen isotope composition of the seep carbonates (Han et al., 2008; Hu et al., 2014; Feng et al., 2018; Chen et al., 2019; Deng et al., 2021; Wei et al., 2020, 2022, 2023). Assuming that the seep carbonates were precipitated in bottom water with a temperature of 8.2°C and the $\delta^{18}O_{seawter}$ value of bottom water is 0‰ SMOW, the theoretical $\delta^{18}O$ values for carbonates can be calculated as 1.73‰ using the method provided by Kim and O'Neil (1997). Additionally, the ^{18}O value of carbonates is enriched by +0.06‰ for each 1mol% of magnesium carbonate (Tarutani et al., 1969). Therefore, according to the content of $MgCO_3$ in SQW-65 (average 5.77 mol%), the theoretical $\delta^{18}O$ value for carbonates was corrected (1.38‰). In contrast, oxygen isotope values of the studied tubular seep carbonate were mostly higher than this value, showing the characteristics of ^{18}O enrichment (Figure 3). This suggests that the tubular seep carbonate (SWQ-65) was influenced by fluids enriched with ^{18}O during its precipitation. Most studies indicate that the primary origins of ^{18}O-enriched fluids are associated with gas hydrate dissociation and clay dehydration (particularly smectite-illite transformation) (Hesse and Harrison, 1981; Hesse, 2003). However, considering the existence of gas hydrate at shallow a sub-bottom depth in the study area (Feng and Chen, 2015; Feng et al., 2018; Ge et al., 2020), we believe that the ^{18}O-enriched fluids generated by gas hydrate dissociation are the main reason for the ^{18}O enrichment of seep carbonates at the SQW-65 station.

In addition, cold seep carbonates are generally thought to have formed in a reducing environment on the seafloor. This is because during the precipitation of seep carbonates, the SD-AOM can produce large amount of hydrogen sulfide, which eventually leads to the anoxic-sulfide state in seep environments (Hu et al., 2014; Lin et al., 2021; Smrzka et al., 2020, 2021; Miao et al., 2021b, 2022a, 2022b, 2024a, 2024b). Moreover, under this circumstance, the behavior of redox-sensitive and REE will be obviously abnormal, which can help us reconstruct the redox state during the precipitation of seep carbonates (Bayon et al., 2011; Bian et al., 2013; Hu et al., 2014; Wang et al., 2015; Yang et al., 2018; Smrzka et al., 2020, 2021; Wei et al., 2020, 2022). First, the shale-normalized REE patterns (Taylor and McLennan, 1985) of the studied tubular seep carbonate shows moderate intensity MREE enrichment (Figure 6A), which is similar to the characteristics of pore water in typical iron reduction zones (Smrzka et al., 2020). In addition, in the diagram of Ce/Ce*-Pr/Pr* (Figure 6A), no obvious Ce anomaly was found (mainly scattered in Field I), indicating that the carbonates were precipitated in an anoxic environment. This is similar to seep carbonates in Gattis Bay (Wang et al., 2018), the Gulf of Mexico (Hu et al., 2014) and the Qiongdongnan area (Wei et al., 2020, 2022). Moreover, there was obvious U enrichment ($21.3<U_{EF}<240.3$) in the studied tubular seep carbonate, indicating an anoxic environment, and this phenomenon also usually occurs in the iron reduction zone (Algeo and Tribovillard, 2009; Smrzka et al., 2020; Miao et al., 2021a). Therefore, it can be considered that the studied tubular seep carbonate was formed in the iron reduction zone of the reducing environment.

5.2 Formation process of the tubular seep carbonate

Based on the analysis conducted, the tubular seep carbonate under study was precipitated in an anoxic environment and was influenced by the gas hydrate evolution process. However, it has been shown that the precipitation environment of tubular seep carbonates is not invariable due to the influence of seep flux and other factors in the process of methane seep activities (Jin et al., 2021; Liang et al., 2022), which may influence the mineral facies and geochemical characteristics of tubular seep carbonates during their precipitation. Additionally, recent dating of tubular carbonates from the Mediterranean, Campos Basin, and South China Sea has shown that the inner parts of tubular carbonates are generally younger but vertically are the same age (Wirsig et al., 2012; Bayon et al., 2013; Yang et al., 2018). Therefore, we can assume that tubular carbonates are usually formed from the rim to the core. Previously, according to the color difference, we divided the cross-section of the tubular seep carbonate into three zones from the rim to the core: A, B and C, which may represent the three stages of carbonate formation (early, middle, and late) (Figure 2). As carbonate precipitation progresses (from the early to late period), the carbonate content increases gradually, and the content of terrigenous detritus, such as quartz, decreases gradually (Figure 3). In addition, with the increase in the carbonate component in the tubular seep carbonate, its geochemical characteristics also show regular changes: the contents of Ti and total REE (ΣREE) decrease significantly, whereas the Y/Ho ratio and U_{EF} increase significantly (Figure 7). This indicates that precipitation environments are variable for the formation of tubular seep carbonate.

First, in the early stage of carbonate precipitation (C), although large number of bicarbonates are produced by SD-AOM, the bicarbonates do not easily accumulate due to strong diffusion, which may lead to a low rate of carbonate precipitation and the slow formation of carbonates. However, with the formation of the periphery of the tubular seep carbonate, the internal channels also become smaller and the diagenetic environment becomes more closed, which can effectively hinder the diffusion of HCO_3^-. Therefore, when methane flux is constant, HCO_3^- concentration will be more concentrated in the internal channels of the tubular seep carbonate under this scenario, thus accelerating the precipitation of carbonates. Here, we found that with the evolution of the carbonate precipitation process (from the rim to the core), the carbonate content increased significantly, accompanied by a decrease in ΣREE content (Figure 7). This is because the faster the precipitation rate of carbonates, the more unfavorable the incorporation of REE, eventually leading to lower ΣREE content (Wright et al., 1987; Ge et al., 2010). On the other hand, with the evolution of the carbonate precipitation process, the diffusion of H_2S is also weakened. Additionally, a higher H_2S concentration in the late channel will also aggravate the degree of reducing environment (Smrzka et al., 2020; Wei et al., 2020, 2022),

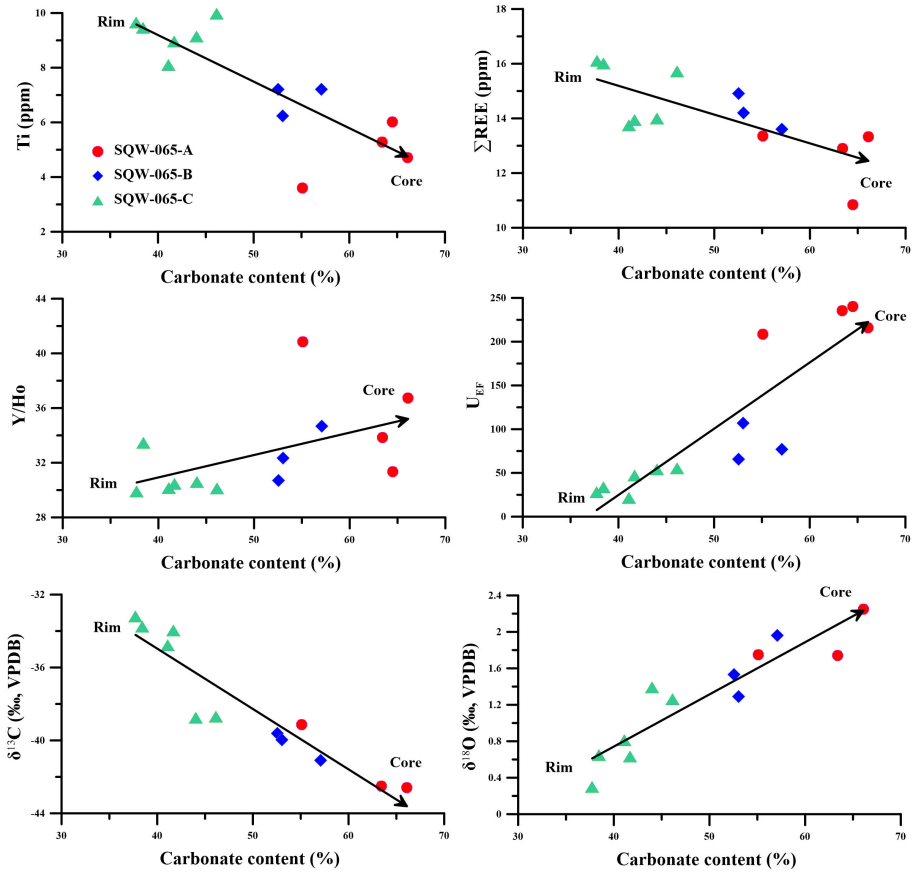

FIGURE 7
Trends of carbonate contents and Ti, ∑REE, Y/Ho, and U_{EF} of the tubular carbonate from the periphery to inner portions.

which leads to an increasing trend in the U_{EF} value in the cross-section of SQW-65 from the rim to the core (Figure 7).

In the early stage of carbonate precipitation (C), carbonate was in direct contact with sediments, and their precipitation process is greatly influenced by terrigenous detritus. Therefore, the tubular seep carbonate formed at this stage contains more terrigenous materials, resulting in a higher content of quartz and Ti (Figures 2, 7). In addition, the low Y/Ho ratio (average 30.8) in the tubular seep carbonate also indicates the influence of terrigenous detritus (25 to 30, Nozaki et al., 1997). Furthermore, the early carbonates of the tubular seep carbonate have a higher ratio of $^{87}Sr/^{86}Sr$ and a lower Sr content (Figures 5, 8), which agrees well with the typical continental component in the sediments in the study area (Wei et al., 2012). However, with the continuous precipitation of the tubular seep carbonate, a carbonate outer wall separated from the sediment was formed, which reduced the influence of terrigenous detritus on the formation of the carbonates. Therefore, in the middle and late stages of carbonate

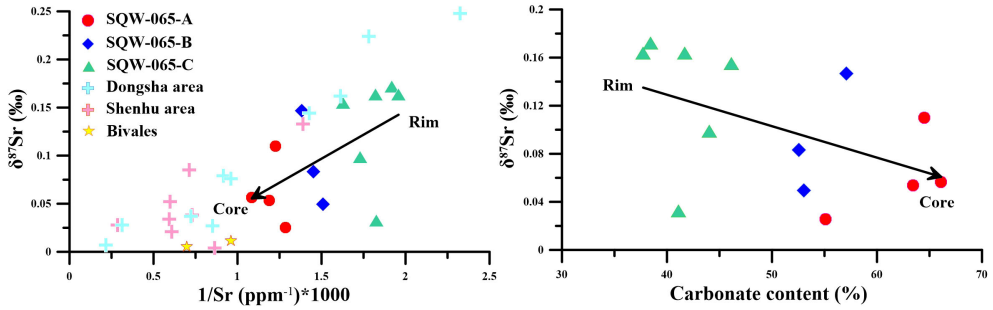

FIGURE 8
$\delta^{87}Sr$-1/Sr*1,000 and $\delta^{87}Sr$-carbonate content diagram of the carbonate samples. Dongsha (Ge et al., 2020), Shenhu (Ge et al., 2020), SQW-65 (this study).

precipitation (B and A), the content of quartz and Ti began to decrease, and the Y/Ho ratio began to increase (Figures 2, 7), which indicated that the influence of terrigenous detritus on carbonate precipitation was weakened. Until the late stage of carbonate formation (A), with the continuous thickening of the carbonate outer walls, they are almost no longer affected by terrigenous detritus. Moreover, in the diagram of δ^{87}Sr-1/Sr, the core of the tubular seep carbonate has a high Sr concentration with a low $^{87}Sr/^{86}Sr$ ratio, which is plotted near the two bivalves (Figure 8). Additionally, the Sr isotopic compositions of bivalves were thought to faithfully replicate the signature of the seawater from which they had precipitated (Hess et al., 1986; Ge et al., 2020). Therefore, this further indicates that the impact of terrigenous detritus on the formation of tubular seep carbonate is diminished.

In addition, the carbon and oxygen isotopic compositions of the studied tubular seep carbonate are also consistent with the above discussion. The results show that $\delta^{18}O$ and $\delta^{13}C$ also present a "covariation" coupling relationship along the cross-section: from the rim to the core, the $\delta^{13}C$ value generally alters from high to low, and the $\delta^{18}O$ value generally alters from low to high with the increase in the carbonate component (Figure 8). Moreover, this regularity has also been found in previous studies of tubular seep carbonate in the northern South China Sea and is thought to be caused by alterations in fluid properties during carbonate precipitation (Jin et al., 2021). With the process of carbonate precipitation, the mixing between the external fluid (^{18}O-poor and ^{13}C-rich) and internal methane seep fluid weakens, resulting in the increase in the $\delta^{18}O$ value and the decrease in the $\delta^{13}C$ value.

In conclusion, we have reconstructed the formation process of tubular seep carbonate based on the mineralogical and geochemical characteristics observed from the outer rim to the core. During the early stages of tubular seep carbonate formation, both seawater and sediment exerted a considerable influence, leading to increased clastic content (Figure 9). However, as the outer wall of the tubular seep carbonate developed, the sedimentary influence became isolated, and the recorded information mainly represented seawater conditions (Figure 9). This finding increases our comprehension of the formation mechanisms and patterns of tubular seep carbonate, highlighting the significance of taking into account the sampling sites when using tubular seep carbonate to reconstruct past marine environments.

5 Conclusion

In this study, we examined tubular seep carbonate samples from the cold seep area in Dongsha, located in the northern South China Sea. These special cold seep carbonates play a significant role in understanding ancient seep activities. Through laboratory experiments, we made significant discoveries regarding the formation and characteristics of these tubular seep carbonates. First, the $\delta^{13}C$ values of the studied tubular seep carbonates were very low. This indicates that the methane present in these carbonates is likely to be of thermogenic origin or a combination of thermogenic and biogenic methane. Additionally, the abnormally positive $\delta^{18}O$ values suggest that the precipitation process of these tubular seep carbonates is influenced by the hydrate dissociation. This highlights the role of hydrate evolution in the formation of these carbonates. Additionally, the shale-normalized REE patterns all displayed no obvious Ce anomalies, accompanied by an obvious enrichment of U, revealing that the carbonates precipitated under anoxic conditions. Subsequently, based on the mineralogical and geochemical characteristics, we identified three distinct stages in the precipitation process of tubular seep carbonates: early, middle, and late stages. As these carbonates precipitate, the influence of terrigenous detritus gradually diminishes, resulting in a more reductive precipitation environment. Overall, our study offers valuable insights into the formation and characteristics of tubular seep carbonates, increasing our understanding of past seepage activities.

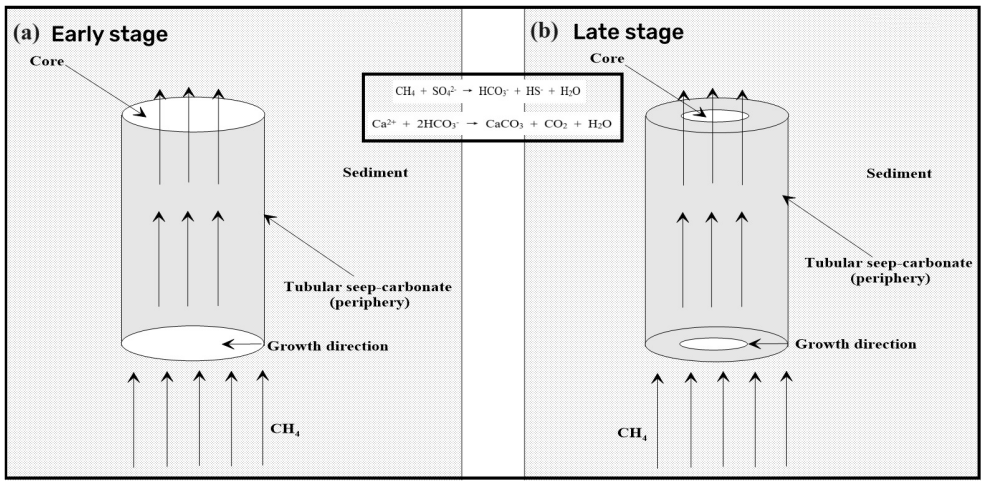

FIGURE 9
Schematic diagram of tubular seep-carbonate formation. **(A)** Early stage. **(B)** Late stage.

Data availability statement

The original contributions presented in the study are included in the article/Supplementary Material. Further inquiries can be directed to the corresponding authors.

Author contributions

JW: Funding acquisition, Resources, Writing – original draft, Writing – review & editing. XM: Conceptualization, Writing – original draft, Writing – review & editing. KG: Data curation, Writing – original draft, Writing – review & editing. JTL: Formal analysis, Investigation, Writing – review & editing. JWL: Investigation, Software, Visualization, Writing – review & editing. XL: Formal analysis, Writing – review & editing. HX: Formal analysis, Writing – review & editing. SC: Investigation, Supervision, Writing – review & editing. KT: Data curation, Investigation, Validation, Writing – review & editing. ZW: Data curation, Methodology, Writing – review & editing. TW: Data curation, Methodology, Writing – review & editing.

Funding

The author(s) declare financial support was received for the research, authorship, and/or publication of this article. This study was supported by the National Natural Science Foundation of China (42276076, 42306080), National Key R&D Program of China (2021YFC2800300), Postdoctoral Fellowship Program of CPSF (GZB20240692), China Geological Survey Project (No. DD20230404), Opening Foundation of Key Lab of Submarine Geosciences and Prospecting Techniques, MOE, and Ocean University of China (SGPT-2023OF-08).

Acknowledgments

We also thank all the crew and participants in the TS07-02&03 expeditions for their support and constructive discussions. Jiangong Wei highly appreciates Mr. Pinxian Wang and Prof Kang Ding for providing the opportunity to participate in the TS07-02&03 research cruise.

Conflict of interest

The authors declare that the research was conducted in the absence of any commercial or financial relationships that could be construed as a potential conflict of interest.

Publisher's note

All claims expressed in this article are solely those of the authors and do not necessarily represent those of their affiliated organizations, or those of the publisher, the editors and the reviewers. Any product that may be evaluated in this article, or claim that may be made by its manufacturer, is not guaranteed or endorsed by the publisher.

Supplementary material

The Supplementary Material for this article can be found online at: https://www.frontiersin.org/articles/10.3389/fmars.2024.1451624/full#supplementary-material

References

Algeo, T., and Tribovillard, N. (2009). Environmental analysis of paleoceanographic systems based on molybdenum–uranium covariation. *Chem. Geol.* 268, 211–225.

Argentino, C., Lugli, F., Cipriani, A., Conti, S., and Fontana, D. (2019). A deep fluid source of radiogenic Sr and highly dynamic seepage conditions recorded in Miocene seep carbonates of the northern Apennines (Italy). *Chem. Geol.* 522, 135–147. doi: 10.1016/j.chemgeo.2019.05.029

Bayon, G., Birot, D., Ruffine, L., Caprais, J.-C., Ponzevera, E., Bollinger, C., et al. (2011). Evidence for intense REE scavenging at cold seeps from the Niger Delta margin. *Earth Planetary Sci. Lett.* 312, 443–452. doi: 10.1016/j.epsl.2011.10.008

Bayon, G., Dupré, S., Ponzevera, E., Etoubleau, J., Chéron, S., Pierre, C., et al. (2013). Formation of carbonate chimneys in the Mediterranean Sea linked to deep-water oxygen depletion. *Nat. Geosci.* 6, 755–760. doi: 10.1038/ngeo1888

Bian, Y., Feng, D., Roberts, H. H., and Chen, D. (2013). Tracing the evolution of seep fluids from authigenic carbonates: Green Canyon, northern Gulf of Mexico. *Mar. Petroleum Geology* 44, 71–81. doi: 10.1016/j.marpetgeo.2013.03.010

Boetius, A., Ravenschlag, K., Schubert, C. J., Rickert, D., Widdel, F., Gieseke, A., et al. (2000). A marine microbial consortium apparently mediating anaerobic oxidation of methane. *Nature* 407, 623–626. doi: 10.1038/35036572

Campbell, K. A., Francis, D. A., Collins, M., Gregory, M. R., Nelson, C. S., Greinert, J., et al. (2008). Hydrocarbon seep-carbonates of a Miocene forearc (East coast basin), north island, new Zealand. *Sediment. Geol.* 204, 83–105. doi: 10.1016/j.sedgeo.2008.01.002

Chen, F., Wang, X., Li, N., Cao, J., Bayon, G., Peckmann, J., et al. (2019). Gas hydrate dissociation during sea-level highstand inferred from U/Th dating of seep carbonate from the South China Sea. *Geophysical Res. Lett.* 46, 13928–13938. doi: 10.1029/2019GL085643

Deng, Y., Chen, F., Guo, Q., Hu, Y., Chen, D., Yang, S., et al. (2021). Possible links between methane seepages and glacial-interglacial transitions in the South China Sea. *Geophysical Res. Lett.* 48, e2020GL091429. doi: 10.1029/2020GL091429

Dickens, G. R., Castillo, M. M., and Walker, J. C. G. (1997). A blast of gas in the latest Paleocene: simulating first-order effects of massive dissociation of oceanic methane hydrate. *Geology*. 25, 259–262. doi: 10.1130/0091-7613(1997)025<0259:ABOGIT>2.3.CO;2

Feng, D., and Chen, D. (2015). Authigenic carbonates from an active cold seep of the northern South China Sea: New insights into fluid sources and past seepage activity. *Deep Sea Res. Part II: Topical Stud. Oceanography* 122, 74–83. doi: 10.1016/j.dsr2.2015.02.003

Feng, D., Peng, Y., Bao, H., Peckmann, J., Roberts, H., and Chen, D. (2016). A carbonate-based proxy for sulfate-driven anaerobic oxidation of methane. *Geology* 44, 999–1002. doi: 10.1130/G38233.1

Feng, D., Qiu, J.-W., Hu, Y., Peckmann, J., Guan, H., Tong, H., et al. (2018). Cold seep systems in the South China Sea: An overview. *J. Asian Earth Sci.* 168, 3–16. doi: 10.1016/j.jseaes.2018.09.021

Ge, L., Jiang, S., Swennen, R., Yang, T., Yang, J., Wu, N., et al. (2010). Chemical environment of cold seep carbonate formation on the northern continental slope of South China Sea: Evidence from trace and rare earth element geochemistry. *Mar. Geology* 277, 21–30. doi: 10.1016/j.margeo.2010.08.008

Han, X., Suess, E., Huang, Y., Wu, N., Bohrmann, G., Su, X., et al. (2008). Jiulong methane reef: Microbial mediation of seep carbonates in the South China Sea. *Mar. Geology* 249, 243–256. doi: 10.1016/j.margeo.2007.11.012

Han, X., Suess, E., Liebetrau, V., Eisenhauer, A., and Huang, Y. (2014). Past methane release events and environmental conditions at the upper continental slope of the South China Sea: constraints from seep carbonates. *Int. J. Earth Sci.* 103, 1873–1887. doi: 10.1007/s00531-014-1018-5

Han, X., Yang, K., and Huang, Y. (2013). Origin and nature of cold seep in northeastern Dongsha area, the South China Sea: Evidence from chimney-like seep carbonates. *Chin. Sci. Bull.* 58. doi: 10.1007/s11434-013-5819-x

Hess, J., Bender, M. L., and Schilling, J. G. (1986). Evolution of the ratio of strontium-87 to strontium-86 in seawater from cretaceous to present. *Science* 231, 979–984. doi: 10.1126/science.231.4741.979

Hesse, R. (2003). Pore water anomalies of submarine gas-hydrate zones as tool to assess hydrate abundance and distribution in the subsurface: What have we learned in the past decade? *Earth-Science Rev.* 61, 149–179. doi: 10.1016/S0012-8252(02)00117-4

Hesse, R., and Harrison, W. E. (1981). Gas hydrates (clathrates) causing pore-water freshening and oxygen isotope fractionation in deep-water sedimentary sections of terrigenous continental margins. *Earth Planetary Sci. Lett.* 55, 453–462. doi: 10.1016/0012-821X(81)90172-2

Hesselbo, S. P., Grocke, D. R., Jenkyns, H. C., Bjerrum, C. J., Farrimond, P., Morgans, B., et al. (2000). Massive dissociation of gas hydrate during a Jurassic oceanic anoxic event. *Nature* 406, 392–395. doi: 10.1038/35019044

Hill, T. M., Kennett, J. P., and Valentine, D. L. (2004). Isotopic evidence for the incorporation of methane-derived carbon into foraminifera from modern methane seeps, Hydrate Ridge, Northeast Pacific. *Geochimica Cosmochimica Acta* 68, 4916–4627. doi: 10.1016/j.gca.2004.07.012

Hu, Y., Feng, D., Peckmann, J., Roberts, H. H., and Chen, D. (2014). New insights into cerium anomalies and mechanisms of trace metal enrichment in authigenic carbonate from hydrocarbon seeps. *Chem. Geol.* 381, 55–66. doi: 10.1016/j.chemgeo.2014.05.014

Huang, H., Feng, D., Guo, Y., Wang, X., Gong, S., Peckmann, J., et al. (2022). Organoclastic sulfate reduction in deep-buried sediments: Evidence from authigenic carbonates of the Gulf of Mexico. *Chem. Geol.* 610, 121094.

Ge, L., Chen, W., Zhu, B., Fan, M., Yang, T., and Jiang, S.. (2020). Sr and Nd isotopes of cold seep carbonates from the northern South China Sea as proxies for fluid sources. *Mar. Pet. Geol.* 115, 104284. doi: 10.1016/j.marpetgeo.2020.104284

Jin, M., Feng, D., Huang, K., Peckmann, J., Li, N., Huang, H., et al. (2021). Behavior of Mg isotopes during precipitation of methane-derived carbonate: Evidence from tubular seep carbonates from the South China Sea. *Chem. Geology* 567, 120101.

Joseph, C., Campbell, K. A., Torres, M. E., Martin, R. A., Pohlman, J. W., Riedel, M., et al. (2013). Methane-derived authigenic carbonates from modern and paleoseeps on the Cascadia margin: Mechanisms of formation and diagenetic signals. *Palaeogeogr. Palaeoclimatol. Palaeoecol.* 390, 52–67. doi: 10.1016/j.palaeo.2013.01.012

Joshi, R. K., Mazumdar, A., Peketi, A., Ramamurty, P. B., Naik, B. G., Kocherla, M., et al. (2014). Gas hydrate destabilization and methane release events in the Krishna–Godavari Basin, Bay of Bengal. *Mar. Pet. Geol.* 58, 476–489. doi: 10.1016/j.marpetgeo.2014.08.013

Kennett James, P., Cannariato Kevin, G., Hendy Ingrid, L., and Behl Richard, J. (2000). Carbon isotopic evidence for methane hydrate instability during quaternary interstadials. *Science* 288, 128–133. doi: 10.1126/science.288.5463.128

Kim, S.-T., and O'Neil, J. R. (1997). Equilibrium and nonequilibrium oxygen isotope effects in synthetic carbonates. *Geochimica Cosmochimica Acta* 61, 3461–3475. doi: 10.1016/S0016-7037(97)00169-5

Kim, S.-T., O'Neil, J. R., Hillaire-Marcel, C., and Mucci, A. (2007). Oxygen isotope fractionation between synthetic aragonite and water: influence of temperature and Mg2 + concentration. *Geochimica Cosmochimica Acta* 71, 4704–4715. doi: 10.1016/j.gca.2007.04.019

Li, C. F., Li, X. H., Li, Q. L., Guo, J. H., and Yang, Y. H. (2012). Rapid and precise determination of sr and nd isotopic ratios in geological samples from the same filament loading by thermal ionization mass spectrometry employing a single-step separation scheme. *Analytica Chimica Acta* 727, 54–60. doi: 10.1016/j.aca.2012.03.040

Liang, Q., Hu, Y., Feng, D., Peckmann, J., Chen, L., Yang, S., et al. (2017). Authigenic carbonates from newly discovered active cold seeps on the northwestern slope of the South China Sea: Constraints on fluid sources, formation environments, and seepage dynamics. *Deep-Sea Res. Part I: Oceanographic Res. Papers* 124, 31–41. doi: 10.1016/j.dsr.2017.04.015

Liang, Q., Huang, H., Sun, Y., Gong, S., Wang, X., Xiao, X., et al. (2022). New insights into the archives of redox conditions in seep carbonates from the Northern South China Sea. *Front. Mar. Sci.* 9, 945908. doi: 10.3389/fmars.2022.945908

Lin, Z., Sun, X., Strauss, H., Eroglu, S., Bottcher, M. E., Lu, Y., et al. (2021). Molybdenum isotope composition of seep carbonates – Constraints on sediment biogeochemistry in seepage environments. *Geochimica Cosmochimica Acta* 307, 56–71. doi: 10.1016/j.gca.2021.05.038

Liu, X., Wang, H., Liu, J., and Zhuang, G. (2024). Microbial sulfate reduction and its role in carbon sequestration in marine sediments. *J. Earth Sci.* 35, 1378–1381. doi: 10.1007/s12583-024-1998-4

Liu, Z., Zhao, Y., Colin, C., Stattegger, K., Wiesner, M. G., Huh, C.-A., et al. (2016). Source-to-sink transport processes of fluvial sediments in the South China Sea. *Earth-Science Rev.* 153, 238–273. doi: 10.1016/j.earscirev.2015.08.005

Mazumdar, A., Dewangan, P., João, H. M., Peketi, A., Khosla, V. R., Kocherla, M., et al. (2009). Evidence of paleo-cold seep activity from the bay of Bengal, offshore India. *Geochem.Geophys. Geosyst.* 10, Q06005. doi: 10.1029/2008GC002337

Miao, X., Feng, X., Li, J., and Lin, L. (2021a). Tracing the paleo-methane seepage activity over the past 20,000years in the sediments of Qiongdongnan Basin, Northwestern South China Sea. *Chem. Geol.* 559, 119956. doi: 10.1016/j.chemgeo.2020.119956

Miao, X., Feng, X., Li, J., Liu, X., Liang, J., Feng, J., et al. (2022a). Enrichment mechanism of trace elements in pyrite under methane seepage. *Geochem. Persp. Let.* 21, 18–22. doi: 10.7185/geochemlet.2211

Miao, X., Feng, X., Liu, X., Li, J., and Wei, J. (2021b). Effects of methane seepage activityon the morphology and geochemistry of authigenic pyrite. *Mar. Petroleum Geology*. doi: 10.1016/j.marpetgeo.2021.105231

Miao, X., Liu, X., Li, Q., Li, A., Cai, F., Kong, F., et al. (2022b). Porewater geochemistry indicates methane seepage in the Okinawa Trough and its implications for the carbon cycle of the subtropical West Pacific. *Palaeogeography Palaeoclimatology Palaeoecol.* 607, 111266. doi: 10.1016/j.palaeo.2022.111266

Miao, X., Oppo, D., Wei, J., Li, Z., Liu, X., Wu, T., et al. (2024a). Enrichment pattern of tungsten in sediments under methane seepage environments: Applicability as a proxy for tracing and reconstructing (paleo-)methane seepage. *Chem. Geology* 663, 122262. doi: 10.1016/j.chemgeo.2024.122262

Miao, X., Wei, J., Li, J., Liu, X., Wang, D., Li, J., et al. (2024b). Isotopically light Mo in sediments of methane seepage controlled by the benthic Fe–Mn redox shuttle process. *Global Planetary Change* 239, 104512. doi: 10.1016/j.gloplacha.2024.104512

Nozaki, Y., Zhang, J., and Amakawa, H. (1997). The fractionation between Y and Ho in the marine environment. *Earth Planetary Sci. Lett.* 148, 329–340. doi: 10.1016/S0012-821X(97)00034-4

Oppo, D., Capozzi, R., Picotti, V., and Ponza, A. (2015). A genetic model of hydrocarbon-derived carbonate chimneys in shelfal fine-grained sediments: The enza river field, northern Apennines (Italy). *Mar. Pet. Geol.* 66, 555–565. doi: 10.1016/j.marpetgeo.2015.03.002

Paytan, A., Kastner, M., Martin, E. E., MacDougall, J. D., and Herbert, T. (1993). Marine barite as a monitor of seawater strontium isotope composition. *Nature* 366, 445–449. doi: 10.1038/366445a0

Peckmann, J., Reimer, A., Luth, U., Luth, C., Hansen, B. T., Heinicke, C., et al. (2001). Methane-derived carbonates and authigenic pyrite from the Northwestern Black Sea. *Mar. Geology* 177, 129–150. doi: 10.1016/S0025-3227(01)00128-1

Peckmann, J., and Thiel, V. (2004). Carbon cycling at ancient methane–seeps. *Chem. Geology* 205, 443–467. doi: 10.1016/j.chemgeo.2003.12.025

Rietveld, H. M. (1967). Line profiles of neutron powder-diffraction peaks for structure refinement. *Acta Crystallographica* 22, 151–152. doi: 10.1107/S0365110X67000234

Ruppel, C. D., and Kessler, J. D. (2017). The interaction of climate change and methane hydrates. *Rev. Geophysics* 55, 126–168. doi: 10.1002/2016RG000534

Sackett, W. M. (1978). Carbon and hydrogen isotope effects during the thermocatalytic production of hydrocarbons in laboratory simulation experiments. *Geochimica Cosmochimica Acta* 42, 571–580. doi: 10.1016/0016-7037(78)90002-9

Saunois, M., Bousquet, P., Poulter, B., Bousquet, P., Canadell, J. G., Jackson, R. B., et al. (2016). The global methane budget 2000–2012. *Earth System Sci. Data* 8, 697–751. doi: 10.5194/essd-8-697-2016

Smrzka, D., Feng, D., Himmler, T., Zwicker, J., Hu, Y., Monien, P., et al. (2020). Trace elements in methane-seep carbonates: Potentials, limitations, and perspectives. *Earth-Science Rev.* 208, 103263. doi: 10.1016/j.earscirev.2020.103263

Smrzka, D., Zwicker, J., Lu, Y., Sun, Y., Feng, D., Monien, P., et al. (2021). Trace element distribution in methane-seep carbonates: The role of mineralogy and dissolved sulfide. *Chem. Geology* 580, 120357.

Suess, E. (2005). *RV SONNE cruise report SO 177, Sino-German cooperative project, South China Sea Continental Margin: Geological methane budget and environmental effects of methane emissions and gas hydrates* (IFM-GEOMAR Reports). Available at: http://store.pangaea.de/documentation/Reports/SO177.pdf.

Tarutani, T., Clayton, R. N., and Mayeda, T. K. (1969). The effect of polymorphism and magnesium substitution on oxygen isotope fractionation between calcium carbonate and water. *Geochimica Cosmochimica Acta* 33, 987–996. doi: 10.1016/0016-7037(69)90108-2

Taylor, B., and Hayes, D. E. (1980). "The tectonic evolution of the South China Basin," in *The Tectonic and Geologic Evolution of Southeast Asian Seas and Islands* (AGU), Union, Washington D.C., 89–104.

Taylor, S. R., and McLennan, S. M. (1985). The continental crust: its composition and evolution. *J. Geol.* 94, 57–72.

Tong, H., Feng, D., Cheng, H., Yang, S., Wang, H., Min, A. G., et al. (2013). Authigenic carbonates from seeps on the northern continental slope of the South China Sea: New insights into fluid sources and geochronology. *Mar. Petroleum Geology* 43, 260 271. doi: 10.1016/j.marpetgeo.2013.01.011

Veizer, J., Ala, D., Amzy, K., Bruckschen, P., Buhl, D., Bruhn, F., et al. (1999). 87Sr/86Sr, d13C and d18O evolution of Paleozoic seawater. *Chem. Geology* 161, 59e88.

Wagner, M., Chappaz, A., and Lyons, T. W. (2017). Molybdenum speciation and burial pathway in weakly sulfidic environments: Insights from XAFS. *Geochim. Cosmochim. Acta* 206, 18–29. doi: 10.1016/j.gca.2017.02.018

Wang, S., Magalhaes, V. H., Pinheiro, L. M., Liu, J., and Yan, W. (2015). Tracing the composition, fluid source and formation conditions of the methane-derived authigenic carbonates in the Gulf of Cadiz with rare earth elements and stable isotopes. *Mar. Petroleum Geology* 68, 192–205. doi: 10.1016/j.marpetgeo.2015.08.022

Wang, X., Li, N., Feng, D., Hu, Y., Bayon, G., Liang, Q., et al. (2018). Using geochemical characteristics of sediment to infer methane seepage dynamics: a case study from Haima cold seeps of the South China Sea. *J. Asian Earth Sci.* 168, 137–144.

Wei, J., Wu, T., and Miao, X. (2023). A dual role of methane seepage intensity on calcium isotopic fractionation. *Geochem. Persp. Let.* 24, 38–42. doi: 10.7185/geochemlet.2303

Wei, J., Wu, T., Miao, X., and Su, P. (2022). Massive natural gas hydrate dissociation during the penultimate deglaciation (~130 ka) in the South China Sea. *Front. Mar. Sci.* 9. doi: 10.3389/fmars.2022.875374

Wei, J., Wu, T., Zhang, W., Deng, Y., Xie, R., Feng, J., et al. (2020). Deeply buried authigenic carbonates in the Qiongdongnan Basin, South China Sea: implications for ancient cold seep activities. *Minerals* 10. doi: 10.3390/min10121135

Whiticar, M. J. (1999). Carbon and hydrogen isotope systematics of bacterial formation and oxidation of methane. *Chem. Geology* 161, 291–314. doi: 10.1016/S0009-2541(99)00092-3

Wright, J., Schrader, H., and Holser, W. T. (1987). Paleoredox variations in ancient oceans recorded by rare earth elements in fossil apatite. *Geochim. Cosmochim. Acta.* 51, 631–644.

Wirsig, C., Kowsmann, R. O., Miller, D. J., de Oliveira Godoy, J. M., and Mangini, A. (2012). U/Th-dating and post-depositional alteration of a cold seep carbonate chimney from the Campos basin offshore Brazil. *Mar. Geol.* doi: 10.1016/j.margeo.2012.10.001

Xie, X., Müller, R., Li, S., Gong, Z., and Bernhard, S. (2006). Origin of anomalous subsidence along the Northern South China Sea margin and its relationship to dynamic topography. *Mar. Petroleum Geology* 23, 745–765. doi: 10.1016/j.marpetgeo.2006.03.004

Yang, K., Chu, F., Zhu, Z., Dong, Y., Yu, X., Zhang, W., et al. (2018). Formation of methane-derived carbonates during the last glacial period on the northern slope of the South China Sea. *J. Asian Earth Sci.* 168, 173–185. doi: 10.1016/j.jseaes.2018.01.022

Zhang, W., and Hu, Z. C. (2020). Estimation of isotopic reference values for pure materials and geological reference materials. *At. Spectrosc* 41, 93–102. doi: 10.46770/AS

Zhang, W., Hu, Z. C., and Liu, Y. S. (2020). Iso-Compass: new freeware software for isotopic data reduction of LA-MC-ICP-MS. *J. Anal. At. Spectrom* 35, 1087–1096. doi: 10.1039/D0JA00084A

Zwicker, J., Smrzka, D., Gier, S., Goedert, J. L., and Peckmann, J. (2015). Mineralized conduits are part of the uppermost plumbing system of oligocene methane-seep deposits, Washington state (USA). *Mar. Pet. Geol.* 66, 616–630. doi: 10.1016/j.marpetgeo.2015.05.035